Inorganic Chemistry

Article

pubs.acs.org/IC

Tuning the Electronics of Bis(tridentate)ruthenium(II) Complexes with Long-Lived Excited States: Modifications to the Ligand Skeleton beyond Classical Electron Donor or Electron Withdrawing Group Decorations

Giovanny A. Parada,[†] Lisa A. Fredin,[§] Marie-Pierre Santoni,[†] Michael Jäger,[‡] Reiner Lomoth,[†] Leif Hammarström,[†] Olof Johansson,[†] Petter Persson,[§] and Sascha Ott*[,†]

[†]Ångström Laboratory, Department of Chemistry, Uppsala University, Box 523, SE-75120 Uppsala, Sweden

[‡]Laboratory of Organic and Macromolecular Chemistry, Friedrich-Schiller-Universität Jena, Humboldtstr. 10, D-07743 Jena, Germany

[§]Chemistry Department, Theoretical Chemistry Division, Lund University, Box 124, SE-22100 Lund, Sweden

Supporting Information

ABSTRACT: A series of homoleptic bis(tridentate) $[Ru(L)_2]^{2+}$ (**1**, **3**) and heteroleptic $[Ru(L)(dqp)]^{2+}$ complexes (**2**, **4**) [L = dqxp (**1**, **2**) or dNinp (**3**, **4**); dqxp = 2,6-di(quinoxalin-5-yl)pyridine, dNinp = 2,6-di(*N*-7-azaindol-1-yl)pyridine, dqp = 2,6-di(quinolin-8-yl)pyridine] was prepared and in the case of **2** and **4** structurally characterized. The presence of dqxp and dNinp in **1**−**4** result in anodically shifted oxidation potentials of the $Ru^{3+/2+}$ couple compared to that of the archetypical $[Ru(dqp)_2]^{2+}$ (**5**), most pronounced for $[Ru(dqxp)_2]^{2+}$ (**1**) with a shift of +470 mV. These experimental findings are corroborated by DFT calculations, which show contributions to the complexes' HOMOs by the polypyridine ligands, thereby stabilizing the HOMOs and impeding electron extraction. Complex **3** exhibits an unusual electronic absorption spectrum with its lowest energy maximum at 382 nm. TD-DFT calculations suggest that this high-energy transition is caused by a localization of the LUMO on the central pyridine fragments of the dNinp ligands in **3**, leaving the lateral azaindole units merely spectator fragments. The opposite is the case in **1**, where the LUMO experiences large stabilization by the lateral quinoxalines. Owing to the differences in LUMO energies, the complexes' reduction potentials differ by about 900 mV [$E_{1/2}(\mathbf{1}^{2+/1+}) = -1.17$ V, $E_{c,p}(\mathbf{3}^{2+/1+}) = -2.06$ V vs $Fc^{+/0}$]. As complexes **1**−**4** exhibit similar excited state energies of around 1.80 V, the variations of the lateral heterocycles allow the tuning of the complexes' excited state oxidation strengths over a range of 900 mV. Complex **1** is the strongest excited state oxidant of the series, exceeding even $[Ru(bpy)_3]^{2+}$ by more than 200 mV. At room temperature, complex **3** is nonemissive, whereas complexes **1**, **2**, and **4** exhibit excited state lifetimes of 255, 120, and 1570 ns, respectively. The excited state lifetimes are thus somewhat shortened compared to that of **5** (3000 ns) but still acceptable to qualify the complexes as photosensitizers in light-induced charge-transfer schemes, especially for those that require high oxidative power.

INTRODUCTION

Ruthenium(II) polypyridyl complexes feature outstanding photophysical properties that make them desirable as photosensitizers in a wide range of applications that rely on light-driven electron transfer, e.g. artificial photosynthesis.[1−5] The tris(bidentate)ruthenium(II) complex $[Ru(bpy)_3]^{2+}$ (bpy = 2,2′-bipyridine) has been used extensively for these types of applications due to its long excited state lifetime (τ = 850 ns at room temperature) and high energy of the relaxed ^{3}MLCT state. However, the preparation of supramolecular donor−photosensitizer−acceptor (D−P−A) arrays based on tris(bidentate) ruthenium(II) where donor and acceptor units are covalently bound to different bpy ligands is limited by the lack of stereospecificity in the most common synthetic approaches that results in multiple geometrical isomers.[6] This shortcoming can be avoided by the use of bis(tridentate) ruthenium(II) complexes, e.g., $[Ru(tpy)_2]^{2+}$ (tpy = 2,2′:6′,2″-terpyridine), which possess D_{2d} symmetry that allows the construction of linear dyads and triads via substitution at the 4′-position of the tpy ligands. Unfortunately, practical use of the structural advantages of $[Ru(tpy)_2]^{2+}$-based complexes is limited by short lifetimes of the ^{3}MLCT state at room temperature (τ = 0.25 ns for $[Ru(tpy)_2]^{2+}$) that arise from

Received: January 7, 2013
Published: April 18, 2013

   dx.doi.org/10.1021/ic400009m | *Inorg. Chem.* 2013, 52, 5128−5137

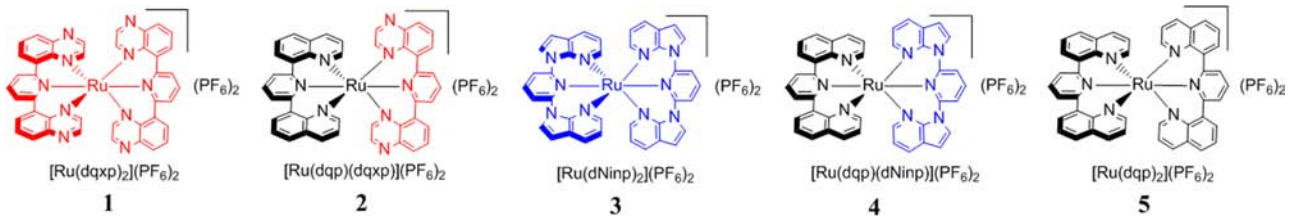

Figure 1. Ruthenium(II) complexes investigated in this study.

efficient thermal population of the ^{3}MC states and subsequent rapid nonradiative decay to the ground state.[7,8] Strategies to prolong the lifetime of the emissive excited state of bis(tridentate) ruthenium(II) complexes have traditionally focused on lowering the energy of the ^{3}MLCT state to disfavor the deactivation pathway via the ^{3}MC state. Such a stabilization of the ^{3}MLCT state can be achieved by introducing electron-withdrawing groups (EWG) or substituents with coplanar aromatic groups that expand the ligands' π-systems. While the excited state lifetimes can sometimes be prolonged considerably with this strategy, lowering of the ^{3}MLCT state inevitably also leads to a decrease of the excited state energy with decreased driving forces for electron transfer in light-driven processes. A second strategy to increase the energy gap between the ^{3}MLCT and ^{3}MC state lies in the destabilization of the ^{3}MC level by increasing the field strength of the ligand. This can be achieved by substitution of the tpy with electron-donor groups (EDG) or the use of anionic ligands with strong σ-donating ability.[9,10] Recently, a combination of these strategies in a bis(tridentate)-ruthenium(II) complex composed of a NHC carbene-based ligand and a 4′-EWG-substituted tpy has resulted in an extended excited state lifetime of ~8 μs at room temperature, the longest ever reported for bis(tridentate)ruthenium(II) complexes.[11]

An alternative approach to increase the ligand field splitting is based on enhanced symmetry around the metal that favors a more octahedral coordination sphere.[12−14] This strategy led to the design of tridentate ligands based on the 2,6-di(quinolin-8-yl)pyridine (dqp) scaffold that give rise to six-membered chelate rings that allow bite angles close to 180° when coordinated to transition metals.[12,15−18] The resulting bis-(tridentate)ruthenium(II) complexes exhibit microsecond excited state lifetimes at room temperature (τ = 3 μs for $[Ru(dqp)_2]^{2+}$).[15] Since the introduction of this concept, different bis(tridentate)ruthenium(II) complexes with six-membered chelate rings have been reported in the literature.[19−21] It is clear, however, that extended bite angles on the tridentate ligand alone do not necessarily ensure long lifetimes of the emissive excited state,[18,21,22] illustrating also the influence of strong electronic effects. Early quantum chemical calculations of $[Ru(dqp)_2]^{2+}$ revealed similar energies of the relaxed ^{3}MLCT and ^{3}MC exited states.[23] Multidimensional excited state analysis confirms this finding and establishes that $[Ru(dqp)_2]^{2+}$ experiences an increased ligand field splitting in the Franck−Condon region *together with* a change in energy and position of the relaxed ^{3}MC state minima; this accounts for the less accessible ^{3}MLCT−^{3}MC crossing point in the excited state potential energy surface, resulting in concomitant extension of the excited state lifetime of the complex.[24,25]

While previous work to alter the electronics of $[Ru(dqp)_2]^{2+}$-based complexes focused on somewhat classical EWG and EDG decorations at the central pyridine of dqp,[26] the present study explores the possibility to tune the electronic properties of the complexes by replacing the lateral quinolinyl subunits of dqp by related heterocyclic ring systems. The strategy has the additional advantage that the 4′-position of the central pyridine is not engaged and is thus available for subsequent chemistry and the attachment of further functional units. 2,6-Di-(quinoxalin-5-yl)pyridine (dqxp) and 2,6-di(*N*-7-azaindol-1-yl)pyridine (dNinp) were identified as interesting ligands to ruthenium due to their expected electronic dissimilarities to dqp. Compared to dqp, the quinoxaline moieties in dqxp are expected to lead to an increased π-acceptor ability of the ligand, while the azaindole derivative should have the opposite effect. Supporting this notion, it has recently been shown in Pt^{II} complexes that replacement of a dqp ligand by a dNinp has led to cathodically shifted oxidation potentials.[22] Both ligands also fulfill the structural requirement that two six-membered chelate rings are formed when coordinated to ruthenium(II). Homoleptic and heteroleptic ruthenium(II) complexes of the ligands dqxp, dNinp, and dqp were thus prepared (Figure 1).

The synthesized complexes were studied by electrochemical and photophysical techniques, and the findings are supported by DFT calculations. It is shown that the redox properties of the ground state and the excited state of **1**−**4** are greatly influenced by the dqxp and dNinp ligands. The excited state of $[Ru(dqxp)_2]^{2+}$ (**1**) exhibits an unusually high oxidative power, making this complex an excellent candidate for thermodynamically challenging photodriven oxidative chemistry.

RESULTS AND DISCUSSION

Synthesis of the Ligands. Different strategies for the synthesis of the three ligands employed in this study are illustrated in Scheme 1. The ligand dqp was prepared in high yield using the Suzuki−Miyaura cross-coupling reaction of quinoline-8-boronic acid and 2,6-dibromopyridine, as reported earlier.[17]

An extension of this methodology (Scheme 1a) to afford dqxp proved more challenging due to the pronounced electrophilicity of the 2- and 3-positions of quinaxoline derivatives. This reactivity precluded the use of organolithium compounds to yield the corresponding boronic acid. Initial attempts to yield dqxp were based on the in situ formation of the 5-substituted boronic acid ester by a Suzuki−Miyaura cross-coupling using bis(pinacolato)diboron and KOAc as base.[27−29] In a subsequent step, the reaction mixture was loaded with 2,6-dibromopyridine, renewed amounts of Pd catalyst/phosphine ligand, and 2 M aqueous Na_2CO_3. This strategy afforded the desired ligand, but with an unsatisfactory isolated yield. Different attempts to optimize this procedure were unsuccessful, and the homocoupling product of the first reaction step was in all cases the major product of the reaction. An alternative strategy that gave the desired cross-coupling reaction between 5-substituted quinoxaline and 2,6-disubstituted pyridine relied on reversing the reactivity of the reactants. This was successfully achieved using 2,6-di(trimethylstannyl)pyridine,[30]

dx.doi.org/10.1021/ic400009m | *Inorg. Chem.* 2013, 52, 5128−5137

Scheme 1. Strategies for the Synthesis of the Ligands dqxp (a) and (b), dNinp (c), and dqp (d)

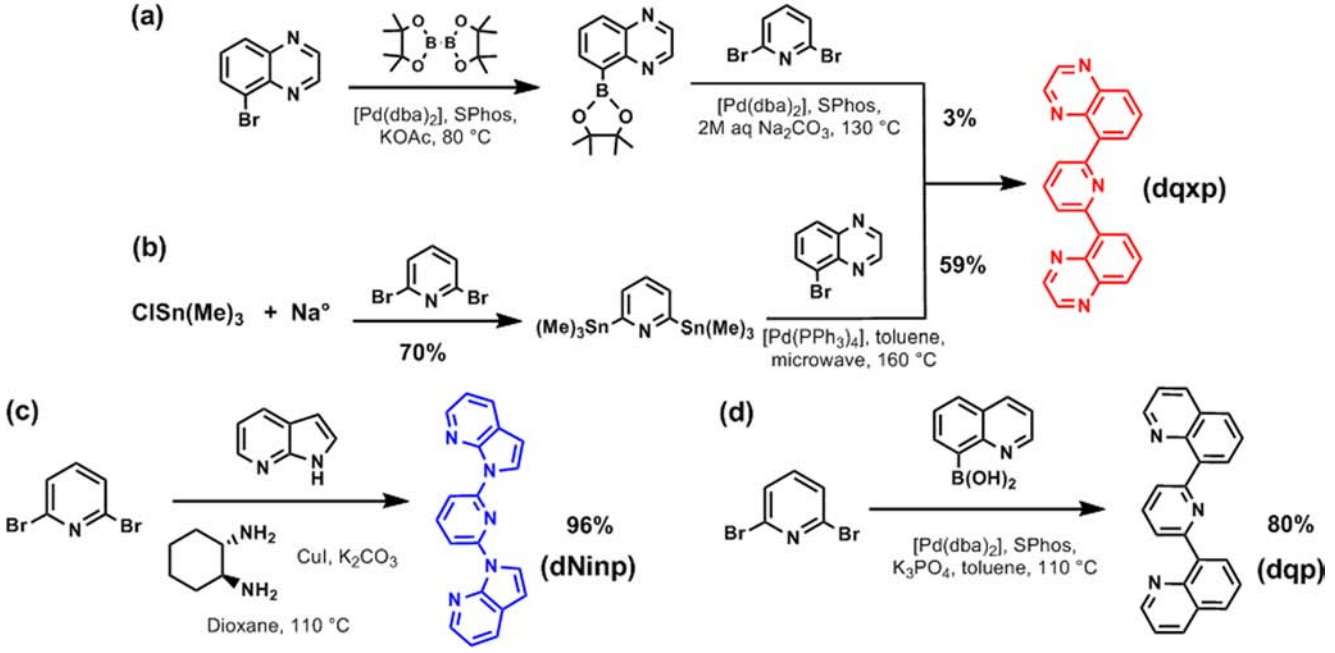

2 equiv of 5-bromoquinoxaline, and tetrakis-(triphenylphosphine)palladium(0) under microwave irradiation. This Stille cross-coupling produced the desired ligand in good yields (Scheme 1b). The ligand dNinp was obtained in high yields by heteroaryl amination according to the procedure established by Garner and co-workers (Scheme 1c).[22]

Synthesis and Characterization of the Ruthenium(II) Complexes. Homoleptic complex **1** was synthesized by reacting 2 equiv of dqxp and $[RuCl_2(DMSO)_4]$ in ethylene glycol, albeit only in modest yield despite extensive efforts to improve the reaction conditions. Heteroleptic complex **2** was prepared by reacting $[Ru(dqp)(CH_3CN)_3](PF_6)_2$[26] and dqxp in ethylene glycol under microwave heating. Temperatures between 180 and 200 °C for 20 min gave the best yields, while longer times and higher temperatures did not improve the conversion and promote the formation of unwanted side products that precipitate upon cooling of the reaction mixture. Synthesis of homoleptic complex **3** required the use of $RuCl_3 \cdot 3H_2O$ as precursor in EtOH at 120 °C using a sealed vial. In a stepwise procedure, $[RuCl_3(dNinp)]$ was first synthesized, followed by removal of the chlorides by the addition of silver nitrate in the presence of a second equivalent of dNinp to give complex **3**. Coordination of a second dNinp occurs only with modest yield. Heteroleptic complex **4** was synthesized in a similar fashion to complex **2**. Best yields were obtained at temperatures between 200 and 210 °C over a period of 80 min. Higher temperatures with shorter reaction times led to formation of multiple undesired products.

A comparison between the ^{1}H NMR spectra of complexes **2** and **5** reveals that the substitution of one dqp ligand by one dqxp has a rather small effect on the chemical shifts of the conserved second dqp. Similarly, substitution of the second dqp by a second dqxp does not induce great changes to the ^{1}H NMR signals of the first dqxp ligand. The ^{1}H NMR chemical shifts of **1** are generally shifted downfield compared to those of **5** (see Figure S8 in the Supporting Information for details). The situation, however, looks more dramatic when comparing the ^{1}H NMR spectra of **3** and **4** with that of **5**. Substitution of the first dqp by dNinp leads to a sizable shielding of the remaining dqp in **4**. Similarly, introduction of the second dNinp (as in **3**) induces shielding effects on the ^{1}H NMR signals of the first dNinp ligand, and the ^{1}H NMR chemical shifts of **3** are generally in a similar region as those of **5** (see Figure S9 in the Supporting Information for details). The various shielding and deshielding effects when comparing the NMR spectra of the complexes can be explained by a number of factors. Electronic effects of the newly introduced ligands through the ruthenium center are operating at the same time as intramolecular π-stacking interactions occur. The latter have been investigated in quite some depth for $[Ru(dqp)_2]^{2+}$-based complexes.[17,31,32] The rather different oxidation potentials among **1**, **2**, and **5** (vide infra) point toward an electronic effect through the metal center, while the rather similar oxidation potentials among **3**, **4**, and **5** suggest π-stacking interactions to be responsible for the large variations in ^{1}H NMR chemical shifts. The exact origin and cause of the NMR chemical shifts are however difficult to assign.

Structures of Complexes 1–4, by X-ray Crystallography and DFT Calculations. Single crystals of heteroleptic complexes **2** and **4** suitable for X-ray diffraction could be grown by slow diffusion of diethyl ether into acetonitrile solutions. The solid-state structures of both complexes show almost perfect octahedral coordination spheres of the six nitrogen donor atoms around the ruthenium metal center due to the six-membered chelate ring size promoted by dqp, dqxp and dNinp (Figure 2a,b). The crystal structures also disclose a helical folding of the dqxp and dNinp ligands around the ruthenium-(II) metal ion (Figure 2c,d) in analogy to the situation in **5**.[17,26] The dihedral angles between the central pyridines and the quinoxalines in dqxp, and the central pyridines and the azaindols in dNinp are 36.4(4)° and 39.7(6)°, respectively, and thus very similar to the dihedral angle observed for dqp in **5**.[17] Strong intramolecular π-stacking interactions are observed in both heteroleptic compounds, with distances between the quinoline and quinoxaline subunits of 3.50 Å for **2** and 3.66 Å between the quinoline and azaindol subunits for **4**.[33] Table 1

dx.doi.org/10.1021/ic400009m | Inorg. Chem. 2013, 52, 5128–5137

Table 1. Selected Bond Lengths and Angles Taken from Single Crystal X-ray Diffraction for 2, 4 and 5,[15] and Selected Computational Results from Geometry Optimizations of 1, 3, and 5[a]

	1_{calc}	2_{exp}		3_{calc}	4_{exp}		5_{exp}	5_{calc}
	dqxp	dqp	dqxp	dNinp	dqp	dNinp	dqp	dqp
N_c–Ru (Å)	2.061	2.033(4)	2.021(4)	2.104	2.029(3)	2.083(3)	2.025(17)	2.049
N_L–Ru (Å)	2.071	2.067(2)	2.050(3)	2.080	2.065(3)	2.064(3)	2.077(16)	2.084
dihedral angles (deg)	36.7	37.4(4)	36.4(4)	38.8	40.3(6)	39.7(6)	39	37.6
N_L–Ru–N_L angle (deg)	179.9	197.4(1)	179.8(1)	179.8	178.78(13)	178.19(14)	177.6(7)	179.5

[a]Calculated bond lengths for the central pyridine to ruthenium (N_c–Ru), and lateral heterocycles to ruthenium (N_L–Ru), as well as dihedral angles and bite angles (N_L–Ru–N_L). Values from geometry optimizations using PBE0/6-31G(d,p) in a polarizable continuum model (PCM) solvent description of an acetonitrile environment.

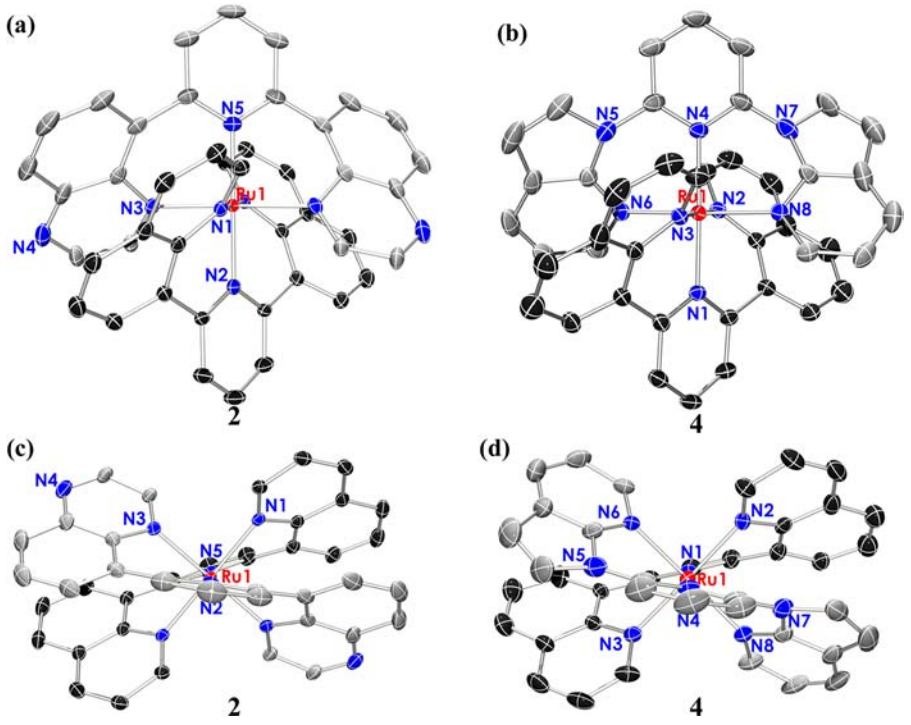

Figure 2. ORTEP views (50% probability ellipsoids) of **2** and **4**. (a and b) The close to 180° bite angle of the ligands dqxp and dNinp in **2** and **4**, respectively. (c and d) The helical folding of the ligands dqxp and dNinp around the metal center, in **2** and **4**, respectively, and the stacking interaction of the lateral motifs thereof. Solvent molecules and anions are omitted for clarity. Key crystallographic data of the complexes are summarized in Table 5.

summarizes selected bond lengths and angles for the complexes obtained from single crystal X-ray diffraction.

The molecular structures of the homoleptic complexes **1** and **3** were obtained by density functional theory (DFT) calculations using the PBE0 functional[34−36] together with the standard all-electron 6-31G(d,p) basis set for all light atoms and the SDD ECP basis set for ruthenium.[37] This level of theory is similar to the ones previously used for complex **5** and related bis(tridentate)ruthenium(II) complexes, which have been successfully investigated computationally in recent years.[12,15,23,31,38] No symmetry was imposed in the optimization of the structures, and frequency calculations were employed to confirm that all optimized geometries are local minima. Selected calculations have been carried out using a polarizable continuum model (PCM) description of an acetonitrile solvent environment. All calculations employed the Gaussian09 program.[39] The DFT calculations (Table 1) indicate that complexes **1** and **3** are structurally very similar to the heteroleptic analogues **2** and **4**, as well as to **5**. The N_L–Ru–N_L angles (N_L depicts the nitrogen at the lateral heterocycles, i.e., quinoxaline-*N* in **1** and azaindole-*N* in **3**) are close to 180° also in the homoleptic complexes **1** and **3**, while their ligands exhibit very similar dihedral angles between the central pyridine and the lateral moieties in dqxp and dNinp, respectively. The angles between 35° and 40° are in the same range as those obtained for **2** and **4** by X-ray crystallography. Also, π-stacking interactions between the lateral subunits of the ligands in **1** and **3** are found. Calculated and crystallographic structural studies show significantly longer distances between the ruthenium(II) and the nitrogen in the central pyridine (N_c–Ru), as well as to the coordinating nitrogens in the lateral heterocylces for complexes that feature the dNinp ligand. In particular, the N_c–Ru distance in **3** is considerably elongated compared to the corresponding distance in **1** and **5**.

Electrochemically and Theoretically Determined Redox Properties of Complexes 1–4. All complexes in this study were investigated by cyclic voltammetry (CV) and differential pulse voltammetry (DPV), and the results are summarized in Table 2 (Supporting Information, Figures S10–S12). The CV of each complex displays a reversible oxidation

dx.doi.org/10.1021/ic400009m | Inorg. Chem. 2013, 52, 5128−5137

Table 2. Electrochemically Determined Redox Properties of Complexes 1−4

	$E_{1/2}{}^a$/V (ΔEp^b/mV)					
complex	$Ru^{3+/2+}$	$L^{0/-1}$	$L^{-1/-2}$	$L^{-2/-3}$	$L^{-3/-4}$	calcd adiabatic ionization potential ΔE_{ox} /eV[d]
1	+1.18 (81)	−1.17 (70)	−1.37 (72)	−1.66 (80)	−1.92 (90)	0.57
2	+0.95 (72)	−1.29 (68)	−1.52 (78)			nd
3	+0.79 (75)	−2.06 (−)[c]				0.22
4	+0.74 (72)	−1.73 (89)	−1.92 (−)[c]	−2.09 (−)[c]		nd
5[e]	+0.71 (63)	−1.73 (62)	−1.90			0.00

[a]From CV in 0.1 M $TBAPF_6$, CH_3CN, ν = 0.1 V/s, vs $Fc^{+/0}$. [b]Difference between anodic and cathodic peak potentials. [c]DPV peak potential. [d]Calculated at the ΔSCF level of theory. E_{ox} of complex **5** was set to 0.00 eV, and the E_{ox} of **1** and **3** are relative to that of **5**. [e]Data from ref 12.

that is assigned to the $Ru^{3+/2+}$ couple in analogy to previously studied ruthenium(II) dqp-based complexes.[15] Compared to **5** ($E_{1/2}$ = 0.71 V vs $Fc^{+/0}$), the exchange of one dqp for dqxp as in **2** results in a substantial anodic shift of the $Ru^{3+/2+}$ couple by ∼240 mV ($E_{1/2}$ = 0.95 V vs $Fc^{+/0}$). The effect is additive as the replacement of the second dqp by dqxp leads to an additional shift of ∼230 mV. The $Ru^{3+/2+}$ couple of **1** is thus shifted by almost 500 mV to more positive potential compared to that of **5**, making oxidized complex **1** a significantly more powerful oxidant than many other bis(tridendate)ruthenium(II) complexes.[26] This additive anodic shift of the $Ru^{3+/2+}$ couple in **1** and **2** relative to complex **5** is analogous to that observed in the series of tris(bidentate)ruthenium(II) complexes $[Ru(bpz)_n(bpy)_{3-n}]^{2+}$, n = 1−3 (bpz = 2,2′-bipyrazine, bpy = 2,2′-bipyridine), in which replacement of each bpy for a bpz shifts the redox potential of the $Ru^{3+/2+}$ couple by ca. 240 mV (from 1.27 V in $[Ru(bpy)_3]^{2+}$ to 1.98 V in $[Ru(bpz)_3]^{2+}$, vs SCE).[40] Replacing the dqp ligand with dNinp in the homoleptic and heteroleptic complexes **3** and **4**, respectively, has a much smaller impact on the $Ru^{3+/2+}$ couple, which is shifted anodically by 80 and 30 mV, respectively, compared to that of **5**. It is interesting to note, however, that the observed anodic shift is opposite to what has been reported for the introduction of dNinp in platinum(II) complexes, where the replacement of a dqp in $[Pt(dqp)Cl]^+$ by dNinp resulted in a *cathodic* shift of 50 mV.[22] The cathodic shift of the metal-based oxidation in the Pt system was rationalized by an increased π-donor ability of this ligand compared to that of dqp. It is thus clear that additional effects must be operational in **3** that compensate for the difference in π-donor ability between dqp and dNinp.

From an inspection of the cathodic scans, it becomes evident that the potentials for the dqxp-containing complexes are generally anodically shifted compared to those that contain dqp and dNinp. Complex **1** shows four reversible one-electron reductions with the first one being anodically shifted by ∼560 mV relative to that of **5.** Complex **2** exhibits two reversible one-electron reductions, the first one being anodically shifted by ∼440 mV relative to that of **5**. In comparison, complex **3** is reduced at much harsher potential, consistent with the electron-rich character of dNinp. This property may also explain the irreversible nature of the reduction process, which leads to the buildup of surface adsorbed material, the oxidation of which can be observed in the reverse scan (Supporting Information, Figure S11). The first reduction of complex **4** occurs at similar potential as that of **5**, supporting the notion that this reduction is mainly centered on the dqp ligand.

Adiabatic ionization potentials (IP_a) have been calculated at the ΔSCF level for complexes **1**, **3**, and **5** using a polarizable continuum model (PCM) description of an acetonitrile solvent environment. This molecular property provides computational insight into the ease by which electrons can be extracted from the Ru^{2+} ground state and are thus relevant for understanding the experimental $Ru^{3+/2+}$ redox potentials. The results from the calculations, listed in Table 2 along with corresponding experimental electrochemical data, illustrate that it is more difficult to extract an electron both from complexes **1** and **3** relative to complex **5** by 0.57 and 0.22 eV, respectively. Although somewhat overestimating, the calculated trend clearly corroborates the experimentally found shifts toward more positive oxidation potentials for complexes **1** and **3** compared to that of complex **5** by 0.47 and 0.08 V, respectively. As shown in the graphical frontier molecular orbital representations for complexes **1** and **3** (Figure 3), the highest occupied molecular orbital (HOMO) levels—from which an electron is removed upon oxidation/ionization—contain large Ru 4d contributions consistent with the metal-centered frontier levels of an octahedral transition metal d^6 complex. In both cases, however, a significant delocalization of the HOMO levels onto the ligands can be observed. This behavior is in significant contrast to that of **5**, where the oxidation is almost exclusively metal-centered.[12] Additional contributions from the ligands in **1** and **3** stabilize the complexes' HOMOs and explain their experimentally observed shift of the ground state oxidation potentials to more positive values. It can be noted that the delocalization of the HOMOs in **1** and **3** also differs from the situation in $[Pt(dqp)Cl]^+$ and $[Pt(dNinp)Cl]^+$, where the HOMO does not

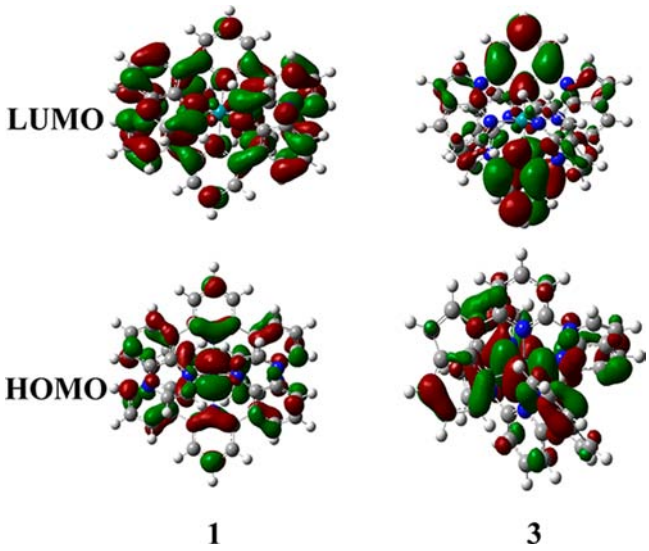

Figure 3. Calculated frontier molecular orbitals of complexes **1** and **3**.

dx.doi.org/10.1021/ic400009m | Inorg. Chem. 2013, 52, 5128−5137

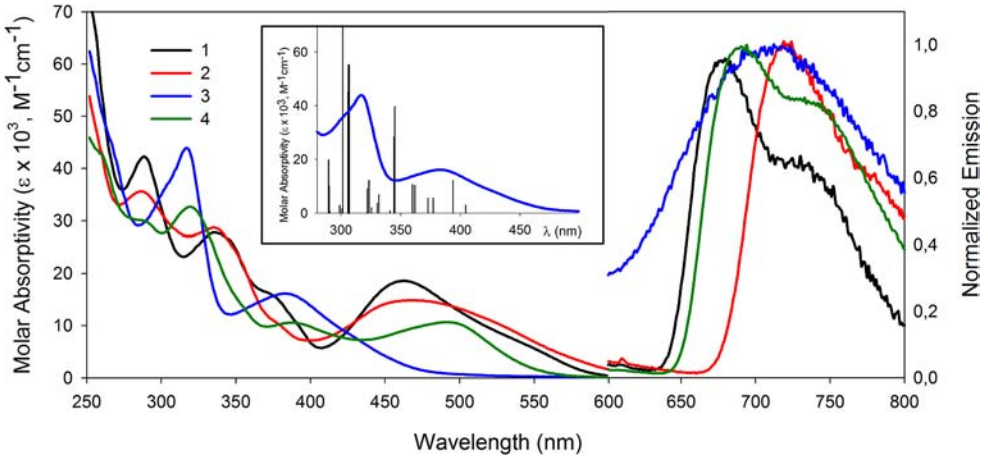

Figure 4. Steady-state absorption spectra at room temperature (CH_3CN) and emission spectra at 77 K (*n*-BuCN) of complexes **1** (black), **2** (red), **3** (blue), and **4** (green). Inset: Experimental absorption spectrum and calculated electronic transitions of **3**.

Table 3. Photophysical Properties of the Complexes 1−4

		Ems/nm				
complex	Abs/nm ($\varepsilon \times 10^{-4}$/$M^{-1}$ cm^{-1})	298 K	77 K[a]	τ/ns	Φ_{em}	E_{0-0}/eV[b]
1	460 (1.8)	715	689	255	~1 × 10^{-3}	1.80
2	465 (1.5)	735	720	120	~6 × 10^{-4}	1.72
3	382 (1.1)		709			1.75
4	493 (1.0)	713	677	1570	~6 × 10^{-3}	1.83
5[c]	490 (1.4)	700	673	3000	0.02	1.84

[a]Emission determined in frozen glass matrix in *n*-BuCN. [b]Estimated from the emission maximum at 77 K as E_{0-0} = 1240 nm/λ_{max} (eV). [c]Data from ref 12.

involve the polypyridine ligand but is localized on the Pt−Cl unit.[22]

Photophysical Properties of Complexes 1−4. UV/vis absorption spectra of complexes **1**−**4** in CH_3CN (Figure 4) show strong transitions in the UV region between 200 and 250 nm and somewhat weaker ones around 260−360 nm. These bands are also observed for the noncoordinated ligands and are assigned to ligand-centered (^{1}LC) transitions. In the visible range, complexes **1** and **2** display strong and broad ^{1}MLCT transitions at 460 nm [ε_{max} = (1.5−1.8) × 10^4 M^{-1} cm^{-1}] (Table 3). Interestingly, complex **3** displays a ^{1}MLCT transition with a strongly blue-shifted absorption maximum at 380 nm (ε_{max} = 1.1 × 10^4 M^{-1} cm^{-1}), whereas **4** features a broad ^{1}MLCT transition with a red-shifted absorption maximum at around 490 nm (ε_{max} = 1.0 × 10^4 M^{-1} cm^{-1}). In order to reveal the reasons for the different absorption features, TD-DFT calculations were performed on the two homoleptic complexes **1** and **3**. Using TD-DFT calculations at the PBE0/6-31G(d,p) level of theory, the experimentally observed large difference of the lowest energy transitions in the UV/vis spectra could be well reproduced (insert in Figure 4 and Supporting Information). While the computational studies reveal multiple transitions beyond 450 nm for complex **1**, no transition at energy lower than 405 nm could be found for **3**. Although the lowest transition energies are well-described by these calculations, the higher energy transitions do not correspond directly with experiment. A detailed analysis of the calculated transitions can be found in the Supporting Information. A simple change of basis set or solvation does not significantly affect the calculated spectra (Supporting Information, Figure S18).

The lowest unoccupied molecular orbitals (LUMO) of complexes **1** and **3** are mainly localized on the dqxp and dNinp ligands, respectively (Figure 3). A closer inspection, however, reveals a significant difference in the distribution of the LUMOs over the two ligands. The major contribution to the LUMO in **1** consists of quinoxaline-based π^* orbitals with high delocalization over these subunits. This situation is very similar to that in **5**,[15] and the orbital contributions to the different electronic transitions can thus be assumed to be very similar in both complexes. The situation, however, changes dramatically in complex **3**, for which the calculated LUMO shows only minor contributions from the azaindolyl subunits, while major contributions arise from the central pyridine π^* orbitals on the dNinp ligand. The decreased delocalization of the LUMO in **3** renders this molecular orbital 1.07 eV higher in energy compared to that of complex **1**, as calculated at the PBE0/6-31G(d,p) level of theory in a PCM description of CH_3CN. The high-energy LUMO also rationalizes the experimentally observed blue-shifted absorption maximum and the cathodically shifted reduction potential in complex **3**. In general, the optical ^{1}MLCT energy gaps also correlate qualitatively with the difference between electrochemically obtained oxidation and reduction potentials ($\Delta E_{1/2} = E_{1/2}^{ox} - E_{1/2}^{red}$), as frequently encountered in other polypyridyl ruthenium(II) complexes.[41,42]

The distribution of the frontier orbitals in space has potential influence on the electronic coupling of the ruthenium(II) complexes to neighboring units in future linear D−P−A arrays. Strong π^* contributions on the two axial pyridyl rings, as seen in particular for the LUMO level of complex **3**, suggest strong electronic coupling to neighboring donor and acceptor units that are covalently bound to the 4′-position. Such strong

dx.doi.org/10.1021/ic400009m | *Inorg. Chem.* 2013, 52, 5128−5137

coupling may be beneficial in future diads and triads utilizing this light-harvesting ruthenium(II) complex.

Emission spectra of the complexes were recorded at room temperature in argon-purged CH_3CN solutions. Complexes **1**, **2**, and **4** display broad emission bands with maxima at 724, 770, and 713 nm, respectively. No emission at room temperature was detected for complex **3**, which may be due to a readily accessible ^{3}MLCT−^{3}MC crossing point in the excited state potential energy surface, probably related to a highly distorted excited state as suggested by the broad emission band disclosed at 77 K (Figure 4). The room temperature excited state lifetimes of **1**, **2**, and **4** in deaerated solutions are on the order of hundreds of nanoseconds, which are very long for bis(tridentate)ruthenium(II) complexes.[43,44]

The excited state energies of complexes **1**−**4** were estimated from the emission maxima of the complexes measured at 77 K in *n*-BuCN glass (Figure 4). The peak with the highest energy in the vibrational progression has been shown to give a good estimate for the exited state energy.[45−47] The excited state energies of **1**−**4** are about 1.80 eV and thus comparable to those of similar dqp-based ruthenium complexes.[26] Considering these generally quite high excited state energies and the strongly anodically shifted redox potentials, complex **1** appears to be a particularly strong excited state oxidant. Using the first reduction potential from the cyclic voltammetry data, the oxidation potential of the excited state of **1** was calculated to be +0.63 V (Table 4). Complex **1** is a stronger excited state oxidant than **5** by more than 500 mV and also stronger than $[Ru(bpy)_3]^{2+}$ by more than 200 mV.[16] Complex **1** is thus an interesting candidate as photosensitizer in applications that require high oxidation power, as for example in water oxidation.[48] Noteworthy is also the fact that the excited state oxidation potentials vary by more than 900 mV between complexes **1** and **3**.

Table 4. Excited State Redox Properties of the Complexes

	$E(PS^{+/*})/V^a$	$E(PS^{*/-})/V^a$
1	−0.62	+0.63
2	−0.77	+0.43
3	−0.96	−0.31
4	−1.09	+0.10
5[b]	−1.13	+0.11
$[Ru(bpy)_3]^{2+}$ [c]	−1.25	+0.39

[a]Estimated as $E^0(PS^{+/*}) \approx E^0(PS^{+/0}) - E_{0-0}$, $E^0(PS^{*/-}) \approx E^0(PS^{0/-}) + E_{0-0}$.[49] [b]Calculated from values taken from ref 12. [c]Calculated from values taken from ref 16.

CONCLUSIONS

In summary, we have shown that modifications of the lateral nitrogen heterocycles on $[Ru(dqp)_2]^{2+}$ (**5**) such as in $[Ru(dqxp)_2]^{2+}$ (**1**) and $[Ru(dNinp)_2]^{2+}$ (**3**) can be used to alter the electronic properties of the complexes substantially. At the same time, the 4′-positions at the central pyridine units are kept untouched, allowing for the future construction of dyads and linearly organized triads. The introduction of dNinp has a profound effect on the LUMO of **3** which is localized to a large extent on the central pyridine unit. As a result, complex **3** is reduced at 330 mV more negative potential compared to **5**. Furthermore, complex **3** exhibits an unusually high-energy ^{1}MLCT optical transition, which could be reproduced and explained by TD-DFT calculations. In contrast, the LUMO of complex **1** contains large contributions of the lateral quinoxaline units, which led to an anodic shift of the reduction potential by 560 meV compared to that of **5**. With comparable excited state energies of around 1.8 eV, the excited state oxidation potentials of complexes **1** and **3** differ by more than 900 mV. From an application perspective, complex **1** offers the highest excited state oxidation power of the series, being 500 mV more oxidizing than **5** and 200 mV stronger than $[Ru(bpy)_3]^{2+}$.

EXPERIMENTAL SECTION

Physical Measurements. NMR spectra were recorded on a JEOL 400 MHz spectrometer at 293 K. Chemical shifts are given in ppm and referenced internally to the residual solvent signal. Microwave heating was performed in an Initiator single mode microwave cavity at 2450 MHz (Biotage). High-resolution ESI-MS were performed on a superconducting 9.4 T FTICR mass spectrometer equipped with an in-house developed emitter. HPLC−MS data were obtained on a Dionex Ultimate 3000 system on a Phenomenex Gemini C18 column (150 × 3.0 mm, 5 μm) coupled to Thermo LCQ Deca XP with electrospray ionization (Supporting Information). Solvents used for HPLC: 0.05% HCO_2H in H_2O and 0.05% HCO_2H in CH_3CN. Electrochemical experiments were performed with a three-electrode setup in a three-compartment cell connected to an Autolab potentiostat with a GPES electrochemical interface (Eco Chemie). The working electrode was a glassy carbon disk (diameter 3 mm, freshly polished). Potentials were measured versus a nonaqueous Ag/Ag^+ reference electrode (CH Instruments, 10 mM $AgNO_3$ in CH_3CN) with a potential of −0.080 V versus the ferrocenium/ferrocene ($Fc^{+/0}$) couple in CH_3CN. UV−vis absorption spectra were measured on a Varian Cary 50 instrument. Steady-state emission measurements were performed on a Fluorolog 3-222 emission spectrometer from Jobin-Yvon and corrected for different detector sensitivity at different wavelengths. Oxygen was removed by purging with argon in the cuvette before and during measurements. Emission spectra and yields at 80 K were measured using a coldfinger setup in a liquid nitrogen filled Dewar flask. Emission yields at room temperature were measured with $[Ru(dqp)_2]^{2+}$ in deoxygenated CH_3CN (Φ_{em} = 0.02) as standard. Time-resolved emission measurements were made with a frequency tripled Q-switched Nd:YAG laser (from Quantel) producing <10 ns flashes. Excitation light at 500 nm was obtained in an OPO. The emission was detected at a right angle with a monochromator and a P928-type PMT. The PMT output was recorded on a Hewlett-Packard digital oscilloscope (2 G samples/s) and analyzed with a nonlinear least-squares algorithm with the Applied Photophysics LKS60 software. All emission measurements were performed in 1 × 1 cm quartz cuvettes in CH_3CN.

X-ray Crystal Structure Analysis. Crystallographic data sets were collected from single crystal samples mounted on a loop fiber and coated with N-paratone oil (Hampton Research). Collection was performed using a Bruker SMART APEX diffractometer equipped with an APEXII CCD detector, a graphite monochromator, and a three-circles goniometer. The crystal-to-detector distance was 5.0 cm, and the data collection was carried out in 512 × 512 pixel mode. The initial unit cell parameters were determined by a least-squares fit of the angular setting of strong reflections, collected by a 10.0° scan in 33 frames over three different parts of the reciprocal space (99 frames total). Cell refinement and data reduction were performed with SAINT V7.68A (Bruker AXS). Absorption correction was done by multiscan methods using SADABS96 (Sheldrick). The structure was solved by direct methods and refined using SHELXL97 (Sheldrick). All non-H atoms were refined by full-matrix least-squares with anisotropic displacement parameters while hydrogen atoms were placed in idealized positions. Refinement of F^2 was performed against all reflections. The weighted *R*-factor *wR* and goodness of fit *S* are based on F^2. Full details concerning the data sets and crystal resolutions can be found in the respective CIF files for **2** and **4**, deposited at the Cambridge Crystallographic Data Centre under

dx.doi.org/10.1021/ic400009m | Inorg. Chem. 2013, 52, 5128−5137

Table 5. Crystallographic Data for the Complexes 2 and 4

compound	2	4
formula	$[C_{44}H_{28}N_{10}Ru](PF_6)_2\cdot(CH_3CN)_2$	$[C_{42}H_{28}N_8Ru][K(NO_3)_3(H_2O)]\cdot CH_3CN$
M_w (g/mol); $F(000)$	1141.86; 2296	1029.99; 2096
T (K); wavelength (Å)	100; 0.71073	100; 0.71073
crystal system	orthorhombic	monoclinic
space group	*Pbcn*	*P*21/*n*
a (Å)	16.7445(16)	11.9736(11)
b (Å)	13.7792(13)	26.443(3)
c (Å)	19.4056(19)	14.2001(14)
β (deg)	90	112.189(1)
V (Å^3); Z; d_{calc} (g/cm^3)	4477.4(7); 4; 1.694	4163.0(7); 4; 1.643
θ range (deg); completeness	1.91−31.18; 0.969	1.54−30.51; 98.4
collected reflectns; R_σ	86 187; 0.0388	78 795; 0.0606
unique reflectns; R_{int}	7026; 0.091	12 504; 0.063
μ (mm^{-1}); abs corr	0.522; semiempirical from equivalents	0.555; semiempirical from equivalents
$R_1(F)$; $wR(F^2)$ $[I > 2\sigma(I)]$	0.0570; 0.1478	0.0667; 0.1826
$R_1(F)$; $wR(F^2)$ (all data)	0.0694; 0.1553	0.0913; 0.1925
GOF(F^2)	1.032	1.106
residual electron density (e$^-$/Å^3)	2.843; −1.678	1.075; −2.402

CCDC 849360 (**2**) and 848070 (**4**). These files can be obtained free of charge from The Cambridge Crystallographic Data Centre via www.ccdc.cam.ac.uk/data_request/cif.

Materials. All commercially available reagents were used as received unless noted otherwise. $[RuCl_2(DMSO)_4]$,[50] 2,6-di(trimethyltin)pyridine,[30] 5-bromoquinoxaline,[51] 2,6-di(quinolin-8-yl)pyridine (dqp),[15] 2,6-di(*N*-7-azaindol-1-yl)pyridine (dNinp),[22] and $[Ru(dqp)(CH_3CN)_3](PF_6)_2$[18] were synthesized by literature methods.

Synthesis of 2,6-Di(trimethylstannyl)pyridine. This compound was synthesized according to the literature procedure.[30] ^{1}H NMR (400 MHz, $CDCl_3$): δ 7.30 ppm (3H, m), 0.31 (18 H, s).

Synthesis of 5-Bromoquinoxaline. This compound was prepared according to the published procedure.[51] ^{1}H NMR (400 MHz, DMSO-d_6): δ 9.07 ppm (1H, d, J = 1.7 Hz), 9.04 (1H, d, J = 1.7 Hz), 8.25 (1H, dd, J = 7.6, 1.1 Hz), 8.14 (1H, dd, J = 8.4, 1.1 Hz), 7.80 (1H, apparent t but dd instead, J = 8.0 Hz).

Synthesis of 2,6-Di(quinolin-8-yl)pyridine (dqp). This compound was prepared according to the published procedure.[15] ^{1}H NMR (400 MHz, $CDCl_3$): δ 9.00 ppm (2H, dd, J = 4.2, 1.9 Hz), 8.28 (2H, dd, J = 7.3, 1.5 Hz), 8.24 (2H, dd, J = 8.4, 1.8 Hz), 8.13 (2H, d, J = 7.8 Hz), 7.96 (1H, t, J = 7.7 Hz), 7.89 (2H, dd, J = 8.3, 1.6 Hz), 7.67 (2H, dd, J = 8.2, 7.3 Hz), 7.46 (2H, dd, J = 8.3, 4.2 Hz). ESI-MS: calcd for $C_{23}H_{15}N_3$ 333.13 au, found $[M + H]^+$ = 334.0 m/z.

Synthesis of 2,6-Di(quinoxalin-5-yl)pyridine (dqxp). 2,6-Di(trimethylstannyl)pyridine (370.0 mg, 0.91 mmol), 5-bromoquinoxaline (415.2 mg, 2.0 mmol), and $[Pd(PPh_3)_4]$ (52.2 mg, 0.044 mmol) were suspended in 5.0 mL of dry toluene. The mixture was purged with argon and heated at 160 °C for 2 h in a sealed microwave vial using microwave irradiation. After cooling, an off-white solid precipitated. The solid was filtrated, washed with cold toluene, and recrystallized twice from hot EtOAc. Yield: 180.4 mg, 59%. ^{1}H NMR (400 MHz, $CDCl_3$): δ 8.92 ppm (2H, d, J = 1.6 Hz), 8.89 (2H, d, J = 1.6 Hz), 8.35 (2H, dd, J = 7.2, 1.2 Hz), 8.35 (2H, dd, J = 8.4, 1.6 Hz), 8.08 (2H, d, J = 7.6 Hz), 7.96 (1H, dd, J = 8.4, 7.2 Hz), 7.90 (2H, dd, J = 8.4, 7.2 Hz) (Supporting Information, Figure S1). ^{13}C NMR (100 MHz, $CDCl_3$): δ 155.7, 144.8, 144.7, 143.3, 143.3, 141.1, 139.5, 135.4, 131.9, 130.3, 130.2. ESI-MS: calcd $C_{21}H_{13}N_5$ 335.12 au, found $[M + H]^+$ = 336 m/z. Anal. Calcd for $C_{21}H_{13}N_5\cdot 0.5$(EtOAc): C, 72.81; H, 4.52; N, 18,46. Found: C, 72.82; H, 4.22; N, 19.62.

Synthesis of 2,6-Di(N-7-azaindol-1-yl)pyridine (dNinp). This compound was prepared according to the published procedure.[22] ^{1}H NMR (400 MHz, $CDCl_3$): δ 8.81 ppm (2H, d, J = 8.1 Hz), 8.44 (2H, d, J = 3.9 Hz), 8.42 (2H, dd, J = 4.8, 1.6 Hz), 8.03 (1H, t, J = 8.1 Hz), 7.96 (2H, dd, J = 7.8, 1.6 Hz), 7.17 (2H, dd, J = 7.8, 4.8 Hz), 6.66 (2H, d, J = 3.9 Hz). ESI-MS: calcd for $C_{19}H_{13}N_5$ 311.1 au, found $[M + H]^+$ = 312.0 m/z.

Synthesis of [Ru(dqp)(CH$_3$CN)$_3$](PF$_6$)$_2$. This compound was prepared according to the published procedure.[18] ^{1}H NMR (acetone-d_6): δ 9.39 (2H, dd, J = 5.1, 1.5 Hz), 8.77 (2H, dd, J = 8.2, 1.5 Hz), 8.74 (2H, dd, J = 7.5, 1.3 Hz), 8.40 (2H, dd, J = 8.2, 1.3 Hz), 8.31 (1H, dd, J = 8.8, 7.2 Hz), 8.21 (2H, m), 8.01 (2H, dd, J = 8.2, 7.5 Hz), 7.77 (2H, dd, J = 8.2, 5.1 Hz), 2.60 (3H, s), 2.18 (6H, s). ESI-MS: calcd for $C_{29}H_{24}F_{12}N_6P_2Ru$ 848.0 au, found $[M - 2CH_3CN - 2PF_6^-]^{2+}$ = 238 m/z, $[M - 2PF_6^-]^{2+}$ = 279 m/z.

*Synthesis of [Ru(dqxp)$_2$](PF$_6$)$_2$ (**1**).* A microwave vial was charged with dqxp (60.1 mg, 0.18 mmol), $[RuCl_2(DMSO)_4]$ (39.4 mg, 0.08 mmol), and ethylene glycol (5 mL); sealed; and heated at 200 °C for 20 min using microwave irradiation. After cooling, the reaction mixture was directly subjected to a column chromatography on silica using $CH_3CN/H_2O/KNO_3$(satd) (40:4:1) as eluent. The chromatographic procedure was done twice, the main red band being collected in each case. The solvents of the fractions containing the product were evaporated in vacuo until dryness and the residue was washed with CH_3CN to remove excess KNO_3. CH_3CN was evaporated in vacuo, and the red solid was redissolved in the minimum amount of water for counteranion exchange using a 10-fold excess of NH_4PF_6, followed by filtration and washing of the formed precipitate with water and Et_2O. The anion exchange was repeated once more using the minimum amount of water/acetone (10:1) to redissolve the solid. The product was dried under vacuum. Yield: 18.7 mg, 22%. ^{1}H NMR (400 MHz, CD_3CN): δ 8.42 ppm (4H, d, J = 2.4 Hz), 8.30 (2H, t, J = 8.2 Hz), 8.06 (4H, d, J = 2.8 Hz), 8.02 (4H, d, J = 8.4 Hz), 7.92 (4H, dd, J = 7.4, 1.2 Hz), 7.87 (4H, dd, J = 8.4, 1.2 Hz), 7.73 (4H, dd, J = 8.4, 7.2 Hz) (Supporting Information, Figure S2). ^{13}C NMR (100 MHz, CD_3CN): δ 155.4, 152.5, 145.3, 140.7, 140.2, 140.0, 133.5, 132.1, 131.3, 130.7, 129.2. ESI-MS: calcd for $C_{42}H_{26}F_{12}N_{10}P_2Ru$ 1062.1 au, found $[M - 2PF_6^-]^{2+}$ 386.1 m/z. Anal. Calcd for $C_{42}H_{26}F_{12}N_{10}P_2Ru\cdot 0.5(Et_2O + CH_3CN)$: C, 48.29; H 2.93; N, 13.14. Found: C, 48.77; H, 2.71; N, 13.59.

*Synthesis of [Ru(dqp)(dqxp)](PF$_6$)$_2$ (**2**).* A microwave vial was charged with dqxp (26.0 mg, 0.077 mmol), $[Ru(dqp)(CH_3CN)_3](PF_6)_2$ (60.8 mg, 0.072 mmol), and ethylene glycol (6 mL); sealed; and heated at 220 °C for 20 min using microwave irradiation. The purification was done as described for $[Ru(dqxp)_2](PF_6)_2$. Yield 22.6 mg, 18%. ^{1}H NMR (400 MHz, CD_3CN): δ 8.34 ppm (2H, d, J = 2.8 Hz), 8.26 (1H, t, J = 8.4 Hz), 8.21 (1H, t, J = 8.2 Hz), 8.20 (2H, d, J = 2.8 Hz), 8.15 (2H, dd, J = 8.4, 1.2 Hz), 7.98 (2H, d, J = 8.0 Hz), 7.93 (2H, d, J = 8.4 Hz), 7.93 (2H, dd, J = 5.2, 1.2 Hz), 7.82 (6H, m), 7.33 (2H, dd, J = 8.4, 1.2 Hz), 7.67 (2H, apparent t but dd instead, J = 8.0 Hz), 7.51 (2H, apparent t but dd instead, J = 8.0 Hz), 7.11 (2H, dd, J = 8.0, 5.2 Hz) (Supporting Information, Figure S3 and ^{1}H−^{1}H COSY in Figure S4). ^{13}C NMR (100 MHz, CD_3CN): δ 159.1, 156.3, 156.0, 152.1, 146.0, 144.7, 141.6, 139.9, 139.3, 139.0, 138.6, 133.7, 132.8, 131.7, 131.7, 131.4, 131.2, 130.2, 128.7, 128.5, 127.3, 126.8, 122.4. ESI-MS: calcd for $C_{44}H_{28}F_{12}N_8P_2Ru$ 1060.07 au, found $[M - 2PF_6^-]^{2+}$ = 385.0 m/z. Anal Calcd for $C_{44}H_{28}F_{12}N_8P_2Ru$: C, 49.87; H, 2.66; N, 10.57. Found: C, 49.61; H, 2.88; N, 9.99. X-ray suitable crystals were obtained from vapor diffusion of Et_2O into a CH_3CN solution.

*Synthesis of [Ru(dNinp)$_2$](PF$_6$)$_2$ (**3**).* A microwave vial was charged with dNinp (76.7 mg, 0.246 mmol), $RuCl_3\cdot(H_2O)_3$ (31.7 mg, 0.121 mmol), and 5 mL of EtOH; sealed; and heated on an oil bath at 120 °C overnight during which a dark precipitate was obtained. $AgNO_3$ (62.0 mg, 0.365 mmol) was added to this reaction mixture and heating at 120 °C was continued for another 16 h. The purification was done as described for $[Ru(dqxp)_2](PF_6)_2$ with collection of the last green band in the chromatographic procedure. Yield: 21.9 mg, 16%. ^{1}H NMR (400 MHz, CD_3CN): δ 8.20 ppm (2H, t, J = 8.3 Hz) 7.88 (4H, dd, J = 7.8, 1,2 Hz), 7.67 (4H, d, J = 4.1 Hz), 7.65 (4H, dd, J = 5.6, 1.2 Hz), 7.49 (4H, d, J = 8.3 Hz), 6.97 (4H, dd, J = 7.8, 5.6 Hz), 6.68 (4H,

dx.doi.org/10.1021/ic400009m | *Inorg. Chem.* 2013, 52, 5128−5137

d, J = 4.0 Hz) (Supporting Information, Figure S5). ^{13}C NMR (100 MHz, CD_3CN): δ 158.7 ppm, 157.9, 151.1, 150.2, 147.4, 142.5, 138.7, 134.6, 131.8, 129.9. ESI-MS: calcd for $C_{38}H_{26}F_{12}N_{10}P_2Ru$ 1018.10 au, found $[M - 2PF_6^-]^{2+}$ = 364.0 m/z.

Synthesis of [Ru(dqp)(dNinp)](PF$_6$)$_2$ (4). A microwave vial was charged with dNinp (22.0 mg, 0.071 mmol), $[Ru(dqp)(CH_3CN)_3](PF_6)_2$ (50.0 mg, 0.060 mmol), and ethylene glycol (2 mL); sealed; and heated at 210 °C for 80 min using microwave irradiation. The purification was done as described for $[Ru(dqxp)_2](PF_6)_2$. Yield: 31.8 mg, 51%. ^{1}H NMR (400 MHz, CD_3CN): δ 8.20 ppm (5H, m) 8.14 (1H, t, J = 8.0 Hz), 7.96 (2H, d, J = 8.1 Hz), 7.94 (2H, dd, J = 7.5, 1.2 Hz), 7.83 (2H, dd, J = 8.2, 1.1 Hz), 7.73 (2H, dd, J = 8.0, 1.2 Hz), 7.52 (2H, d, J = 8.0 Hz), 7.48 (2H, dd, J = 5.2, 1.2 Hz), 7.46 (2H, d, J = 4.0 Hz), 7.38 (2H, d, J = 8.0 Hz), 7.03 (2H, dd, J = 8.0, 5.2 Hz), 6.99 (2H, dd, J = 7.6, 5.6 Hz), 6.55 (2H, d, J = 4.0 Hz) (Supporting Information, Figure S6 and ^{1}H−^{1}H COSY in Figure S7). ^{13}C NMR (100 MHz, CD_3CN): δ 158.7 ppm, 157.9, 151.1, 150.2, 150.2, 147.4, 142.5, 139.1, 138.7, 134.6, 134.2, 131.8, 131.6, 129.9, 129.1, 128.41, 128.4, 122.8, 122.4, 121.9, 116.7, 108.3. ESI-MS: calcd for $C_{42}H_{28}F_{12}N_8P_2Ru$ 1038.07 au, found $[M - 2PF_6^-]^{2+}$ = 374.1 m/z. Anal. Calcd for $C_{42}H_{28}F_{12}N_8P_2Ru$: C, 48.71; H, 2.72; N, 10.82. Found: C, 48.21; H, 3.03; N, 10.91. X-ray suitable crystals were obtained from vapor diffusion of Et_2O into a CH_3CN solution of the nitrate salt of the complex.

■ ASSOCIATED CONTENT

Ⓢ Supporting Information

NMR characterization of 2,6-bis(quinoxalin-5-yl)pyridine (dqxp) and complexes **1**−**4**; electrochemistry of complexes **1**−**4**; emission spectra at room temperature for complexes **1**, **2**, and **4**; crystallographic information of complexes **2** and **4**; calculated DFT optimized coordinates of complexes **1**, **3**, and **5**; and detailed breakdown of metal orbital and molecular orbital contributions to calculated absorption spectra. This material is available free of charge via the Internet at http://pubs.acs.org.

■ AUTHOR INFORMATION

Corresponding Author

*E-mail: sascha.ott@kemi.uu.se.

Notes

The authors declare no competing financial interest.

■ ACKNOWLEDGMENTS

This work was supported by the Swedish Research Council, the Swedish Energy Agency and the Knut and Alice Wallenberg Foundation. P.P. acknowledges support from the NSC and LUNARC supercomputing facilities.

■ REFERENCES

(1) Alstrum-Acevedo, J. H.; Brennaman, M. K.; Meyer, T. J. *Inorg. Chem.* **2005**, *44*, 6802.

(2) Balzani, V.; Credi, A.; Venturi, M. *ChemSusChem* **2008**, *1*, 26.

(3) Sun, L.; Hammarström, L.; Åkermark, B.; Styring, S. *Chem. Soc. Rev.* **2001**, *30*, 36.

(4) Gust, D.; Moore, T. A.; Moore, A. L. *Acc. Chem. Res.* **2009**, *42*, 1890−1898.

(5) Magnuson, A.; Anderlund, M.; Johansson, O.; Lindblad, P.; Lomoth, R.; Polivka, T.; Ott, S.; Stensjö, K.; Styring, S.; Sundström, V.; Hammarström, L. *Acc. Chem. Res.* **2009**, *42*, 1899−1909.

(6) Richard Keene, F. *Coord. Chem. Rev.* **1997**, *166*, 121−159.

(7) Winkler, J. R.; Netzel, T.; Creutz, C.; Sutin, N. *J. Am. Chem. Soc.* **1987**, *109*, 2381.

(8) Calvert, J. M.; Caspar, J. V.; Binstead, R. A.; Westmoreland, T. D.; Meyer, T. J. *J. Am. Chem. Soc.* **1982**, *104*, 6620.

(9) Medlycott, E. A.; Hanan, G. S. *Chem. Soc. Rev.* **2005**, *34*, 133−142.

(10) Medlycott, E. A.; Hanan, G. S. *Coord. Chem. Rev.* **2006**, *250*, 1763.

(11) Brown, D. G.; Sanguantrakun, N.; Schulze, B.; Schubert, U. S.; Berlinguette, C. P. *J. Am. Chem. Soc.* **2012**, *134*, 12354−12357.

(12) Abrahamsson, M.; Jäger, M.; Kumar, R. J.; Österman, T.; Persson, P.; Becker, H.-C.; Johansson, O.; Hammarström, L. *J. Am. Chem. Soc.* **2008**, *130*, 15533.

(13) Abrahamsson, M.; Wolpher, H.; Johansson, O.; Larsson, J.; Kritikos, M.; Eriksson, L.; Norrby, P.-O.; Bergquist, J.; Sun, L.; Åkermark, B.; Hammarström, L. *Inorg. Chem.* **2005**, *44*, 3215.

(14) Wolpher, H.; Johansson, O.; Abrahamsson, M.; Kritikos, M.; Sun, L.; Åkermark, B. *Inorg. Chem. Commun.* **2004**, *7*, 337.

(15) Abrahamsson, M.; Jäger, M.; Österman, T.; Eriksson, L.; Persson, P.; Becker, H.-C.; Johansson, O.; Hammarström, L. *J. Am. Chem. Soc.* **2006**, *128*, 12616.

(16) Hammarström, L.; Johansson, O. *Coord. Chem. Rev.* **2010**, *254*, 2546−2559.

(17) Jäger, M.; Eriksson, L.; Bergquist, J.; Johansson, O. *J. Org. Chem.* **2007**, *72*, 10227.

(18) Jäger, M.; Smeigh, A.; Lombeck, F.; Görls, H.; Collin, J.-P.; Sauvage, J.-P.; Hammarström, L.; Johansson, O. *Inorg. Chem.* **2009**, *49*, 374−376.

(19) Schramm, F.; Meded, V.; Fliegl, H.; Fink, K.; Fuhr, O.; Qu, Z.; Klopper, W.; Finn, S.; Keyes, T. E.; Ruben, M. *Inorg. Chem.* **2009**, *48*, 5677−5684.

(20) Breivogel, A.; Förster, C.; Heinze, K. *Inorg. Chem.* **2010**, *49*, 7052−7056.

(21) Dinda, J.; Liatard, S.; Chauvin, J.; Jouvenot, D.; Loiseau, F. *Dalton Trans.* **2011**, *40*, 3683−3688.

(22) Garner, K. L.; Parkes, L. F.; Piper, J. D.; Williams, J. A. G. *Inorg. Chem.* **2009**, *49*, 476−487.

(23) Borg, O. A.; Godinho, S. S. M. C.; Lundqvist, M. J.; Lunell, S.; Persson, P. *J. Phys. Chem. A* **2008**, *112*, 4470−4476.

(24) Österman, T.; Abrahamsson, M.; Becker, H.-C.; Hammarström, L.; Persson, P. *J. Phys. Chem. A* **2012**, *116*, 1041−1050.

(25) Österman, T.; Persson, P. *Chem. Phys.* **2012**, *407*, 76−82.

(26) Jäger, M.; Kumar, R. J.; Görls, H.; Bergquist, J.; Johansson, O. *Inorg. Chem.* **2009**, *48*, 3228.

(27) Jäger, M. Beyond Classical Ruthenium(II) Polypyridyl Complexes. Ph.D. Thesis, Uppsala University, 2009.

(28) Ishiyama, T.; Itoh, Y.; Kitano, T.; Miyaura, N. *Tetrahedron Lett.* **1997**, *38*, 3447−3450.

(29) Miura, M.; Koike, T.; Ishihara, T.; Hirayama, F.; Sakamoto, S.; Okada, M.; Ohta, M.; Tsukamoto, S.-I. *Synth. Commun.* **2006**, *36*, 3809−3820.

(30) Schubert, U. S.; Eschbaumer, C. *Org. Lett.* **1999**, *1*, 1027−1029.

(31) Österman, T.; Abrahamsson, M.; Becker, H.-C.; Hammarström, L.; Persson, P. *J. Phys. Chem. A* **2012**, *116*, 1041.

(32) Sharma, S.; Lombeck, F.; Eriksson, L.; Johansson, O. *Chem.—Eur. J.* **2010**, *16*, 7078−7081.

(33) Platon routine was used to calculate the interplanar distances between the lateral motifs of the ligands in complexes **2** and **4**.

(34) Perdew, J. P.; Burke, K.; Ernzerhof, M. *Phys. Rev. Lett.* **1996**, *77*, 3865.

(35) Perdew, J. P.; Burke, K.; Ernzerhof, M. *Phys. Rev. Lett.* **1997**, *78*, 1396.

(36) Adamo, C.; Barone, V. *J. Chem. Phys.* **1999**, *110*, 6158.

(37) Dolg, M.; Wedig, U.; Stoll, H.; Preuss, H. *J. Chem. Phys.* **1987**, *86*, 866.

(38) Abrahamsson, M.; Lundqvist, M. J.; Wolpher, H.; Johansson, O.; Eriksson, L.; Bergquist, J.; Rasmussen, T.; Becker, H.-C.; Hammarström, L.; Norrby, P.-O.; Åkermark, B.; Persson, P. *Inorg. Chem.* **2008**, *47*, 3540.

(39) R. A., Frisch, M. J.; Trucks, G. W.; Schlegel, H. B.; Scuseria, G. E.; Robb, M. A.; Cheeseman, J. R.; Scalmani, G.; Barone, V.; Mennucci, B.; Petersson, G. A.; Nakatsuji, H.; Caricato, M.; Li, X.; Hratchian, H. P.; Izmaylov, A. F.; Bloino, J.; Zheng, G.; Sonnenberg, J.

L.; Hada, M.; Ehara, M.; Toyota, K.; Fukuda, R.; Hasegawa, J.; Ishida, M.; Nakajima, T.; Honda, Y.; Kitao, O.; Nakai, H.; Vreven, T.; Montgomery, J. A.; , Jr., Peralta, J. E.; Ogliaro, F.; Bearpark, M.; Heyd, J. J.; Brothers, E.; Kudin, K. N.; Staroverov, V. N.; Kobayashi, R.; Normand, J.; Raghavachari, K.; Rendell, A.; Burant, J. C.; Iyengar, S. S.; Tomasi, J.; Cossi, M.; Rega, N.; Millam, J. M.; Klene, M.; Knox, J. E.; Cross, J. B.; Bakken, V.; Adamo, C.; Jaramillo, J.; Gomperts, R.; Stratmann, R. E.; Yazyev, O.; Austin, A. J.; Cammi, R.; Pomelli, C.; Ochterski, J. W.; Martin, R. L.; Morokuma, K.; Zakrzewski, V. G.; Voth, G. A.; Salvador, P.; Dannenberg, J. J.; Dapprich, S.; Daniels, A. D.; Farkas, O.; Foresman, J. B.; Ortiz, J. V.; Cioslowski, J.; Fox, D. J. *Gaussian 09*; Gaussian, Inc., Wallingford, CT, 2009.

(40) Ross, H. B.; Boldaji, M.; Rillema, D. P.; Blanton, C. B.; White, R. P. *Inorg. Chem.* **1989**, *28*, 1013−1021.

(41) Juris, A.; Campagna, S.; Balzani, V.; Gremaud, G.; Von Zelewsky, A. *Inorg. Chem.* **1988**, *27*, 3652−3655.

(42) Curtright, A. E.; McCusker, J. K. *J. Phys. Chem. A* **1999**, *103*, 7032−7041.

(43) Sauvage, J.-P.; Collin, J.-P.; Chambron, J. C.; Guillerez, S.; Coudret, C.; Balzani, V.; Barigelletti, F.; De Cola, L.; Flamigni, L. *Chem. Rev.* **1994**, *94*, 993−1019.

(44) Maestri, M.; Armaroli, N.; Balzani, V.; Constable, E. C.; Thompson, A. M. W. C. *Inorg. Chem.* **1995**, *34*, 2759−2767.

(45) Treadway, J.; Loeb, B.; Lopez, R.; Anderson, P. A.; Keene, F. R.; Meyer, T. J. *Inorg. Chem.* **1996**, *35*, 2242−2246.

(46) Caspar, J. V.; Meyer, T. J. *Inorg. Chem.* **1983**, *22*, 2444−2453.

(47) Hammarström, L.; Barigelletti, F.; Flamigni, L.; Indelli, M. T.; Armaroli, N.; Calogero, G.; Guardigli, M.; Sour, A.; Collin, J.-P.; Sauvage, J.-P. *J. Phys. Chem. A* **1997**, *101*, 9061−9069.

(48) Duan, L.; Tong, L.; Xu, Y.; Sun, L. *Energy Environ. Sci.* **2011**, *4*, 3296−3313.

(49) Balzani, V.; Bolletta, F.; Gandolfi, M.; Maestri, M. In *Topics in Current Chemistry*; Springer: Berlin, 1978; Vol. 75, pp 1−64.

(50) Evans, I. P.; Spencer, A.; Wilkinson, G. *J. Chem. Soc., Dalton Trans.* **1973**, 204−209.

(51) Brown, W. D.; Gouliaev, A. H. *Synthesis* **2002**, *2002*, 83−86.

dx.doi.org/10.1021/ic400009m | *Inorg. Chem.* 2013, 52, 5128−5137